Volterra-Mapping-Based Behavioral Modeling of Nonlinear Circuits and Systems for High Frequencies

Tianhai Wang, *Member, IEEE,* and Thomas J. Brazil, *Senior Member, IEEE*

***Abstract*—This paper presents and validates a discrete-time/frequency-domain approach to the problem of Volterra-series-based behavioral modeling for high-frequency systems. The proposed technique is based on the acquisition of samples of the input/output data, both of which are sampled at the Nyquist rate corresponding to the input signal. The method is capable of identifying the time-/frequency-domain Volterra kernels/transfer functions of arbitrary causal time-invariant weakly nonlinear circuits and systems operating at high frequencies subject to essentially a general random or multitone excitation. The validity and efficiency of the proposed modeling approach has been demonstrated by several examples in high-frequency applications and good agreement has been obtained between results calculated using the proposed model and results measured or simulated with commercial simulation tools.**

***Index Terms*—Behavioral modeling, high-frequency systems, nonlinear circuits and systems, Volterra series.**

I. Introduction

STIMULATED by the enormous growth in the commercial applications of RF/microwave technologies, computer-aided design (CAD) is becoming a critical enabling technology in the development of modern high-frequency circuits and systems, e.g., in third-generation digital mobile cellular communication systems around 2.0 GHz [1], [2]. Although CAD encompasses a great many aspects of design, it is very important that practical analysis tools demonstrate an efficient simulation speed and they should also provide an accurate modeling environment for the prediction of the nonlinear behavior of RF/microwave circuits and systems.

Due to the advantages of using a behavioral model (also called a "black-box" model) in simulation, it has become an approach recently investigated by many researchers [3]–[5]. In general, the time-domain unit impulse response or its associated frequency-domain transfer function can completely characterize the behavior of any linear time-invariant network, and these can be thought as a form of behavioral model for linear networks. A typical example in the high-frequency regime is provided by the S-parameters of a linear network. For nonlinear networks, however, an extension through an approach such as the Volterra theory has to be used to find an equivalent framework. Volterra series-based behavioral models have been used successfully to solve many problems in science and engineering and this kind of approach is playing an ever-increasing role in recent years [6]–[9]. A critical problem in utilizing Volterra mapping as the basis for a behavioral model is the identification/estimation of the time-domain Volterra kernels or the associated frequency-domain Volterra transfer functions. Several identification algorithms in the frequency-domain have been introduced in earlier work with the assumption of Gaussian inputs [10], Poisson random impulse train inputs [11], or multitone sinusoidal inputs [12]. Although these can lead to a significant simplification of the identification process, the input excitations in the first two cases are assumed to satisfy strict Gaussian or Poisson statistical properties, while the probe method is only valid for certain nonlinear circuits or systems subject to incommensurate multitone sinusoidal input [10]–[12].

Other discrete frequency-domain methods with subsequent improvements [7], [8] have been described, which are more general in the sense that no specific statistical assumption needs be made about the input. However, the sampling frequency must be at least n-times the bandwidth of the input signal for the identification of an nth-order Volterra-series-based nonlinear system. The corresponding computation complexity is increased since, in the first place, large-order discrete Fourier transforms (DFTs) are required under these sampling frequency conditions, and secondly, increased quantities of data samples in blocks are required for the estimation of Volterra transfer functions to meet the minimum mean square error (MMSE) estimate criterion. Furthermore, aliasing effects have been largely ignored in the literature to date when digital methods have been used to identify Volterra kernels for continuous-time nonlinear systems using sampling techniques.

The method proposed in this paper aims to achieve improved performance compared to conventional discrete frequency-domain methods by performing a mixed-domain (time- and frequency-domain) analysis [9]. It seeks to overcome some of the disadvantages of previously reported methods by properly accounting for the aliasing effect under the much more favorable condition of Nyquist sampling of the *input* signal, while also providing greater accuracy by adapting a least squares solution technique with minimally sampled data blocks. Some individual parts of this study have already been briefly outlined in the authors' earlier publications [13]–[16], however, a more

Manuscript received June 30, 2002; revised December 16, 2002. This work was supported under the Enterprise Ireland Strategic Research Program.

T. Wang is with the Department of Corporate Research and Design, Tycoelectronics, M/A-COM Inc., Lowell, MA 01853 USA (e-mail: wangtian@tycoelectronics.com).

T. J. Brazil is with the Department of Electronic and Electrical Engineering, University College Dublin, Dublin 4, U.K. (e-mail: tom.brazil@ucd.ie).

Digital Object Identifier 10.1109/TMTT.2003.810151

systematic and unified discussion of the mathematical basis is provided in this paper. In order to properly describe the basis and range of applicability of the proposed approach, our attention is focused on the Volterra-based modeling of an arbitrary causal time-invariant cubically nonlinear system. This paper is organized as follows. In Section II, we introduce techniques to take account of aliasing effects, which result in improved sampling requirements for nonlinear system identification. In Section III, a mixed-domain analysis is performed to obtain the discrete mixed-domain model. In Section IV, we describe the estimation procedure of the Volterra kernels and transfer functions. Finally, computer simulation and experimentation are presented in Section V.

II. Aliasing Effects and Sampling Requirements

For the numerical identification of a Volterra-mapping-based nonlinear system, the input/output signals must be sampled for further processing. It is well known that a nonlinear system may generate new output frequency components that extend far beyond the input frequency bandwidth. Therefore, in previous studies on nonlinear system identification [6]–[9], the sampling frequency is more than twice the maximum output frequency in order to avoid aliasing effects. However, it is sufficient to sample at twice the maximum *input* frequency for nonlinear system identification if the aliasing effect is taken into account. The details will be demonstrated in this section.

In the discrete time domain, a Volterra-series description of a cubic nonlinearity can be defined using a discrete-time version of the continuous time-domain series as [6]–[9]

$$y(n)=\sum_{i=0}^{+\infty}h_1(i)x(n-i)+\sum_{i=0}^{+\infty}\sum_{j=0}^{+\infty}h_2(i,\,j)x(n-i)x(n-j)+\sum_{i=0}^{+\infty}\sum_{j=0}^{+\infty}\sum_{k=0}^{+\infty}h_3(i,\,j,\,k)x(n-i)\cdot x(n-j)x(n-k)+e(n) \tag{1}$$

where $x(n)$ and $y(n)$ are sampled versions of the continuous-time input/output signals, while $e(n)$ denotes the model error at the time instant nT (T is the sampling time interval and $h_1(i)$, $h_2(i,\,j)$, and $h_3(i,\,j,\,k)$ correspond to the first-, second-, and third-order discrete-time Volterra kernels, respectively).

Suppose an input signal band-limited to half the sampling frequency is applied to this nonlinear system. In the frequency domain, the Volterra model can be described as

$$Y(f)=Y_1(f)+Y_2(f)+Y_3(f) \tag{2}$$

where

$$Y_1(f)=H_1(f)X(f) \tag{3}$$

$$Y_2(f)=T\int_{-1/2T}^{+1/2T}Y_2(f-f_1,\,f_1)\,df_1 \tag{4}$$

$$Y_3(f)=T^2\int_{-1/2T}^{+1/2T}\int_{-1/2T}^{+1/2T}\cdot Y_3(f-f_1,\,f_1-f_2,\,f_2)\,df_1\,df_2 \tag{5}$$

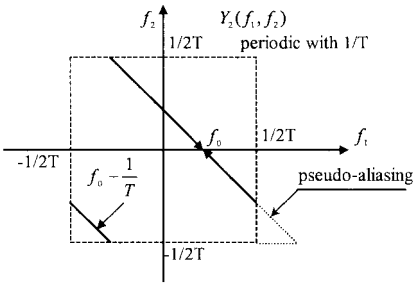

Fig. 1. Illustration of the discrete-time operation that reduces the two-dimensional frequency function Y_2^d to the one-dimensional Fourier transform Y^d of the output signal. In particular, it shows the generation of the output components at f_0.

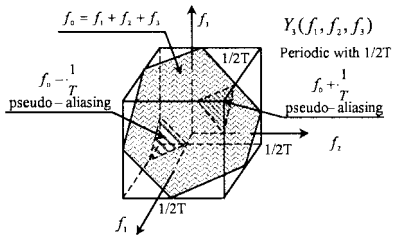

Fig. 2. Illustration of the discrete-time operation that reduces the three-dimensional frequency function Y_3^d to the one-dimensional Fourier transform Y^d of the output signal. In particular it shows the generation of the output components at f_0.

$$Y_2(f_1,\,f_2)=H_2(f_1,\,f_2)X(f_1)X(f_2) \tag{6}$$

$$Y_3(f_1,\,f_2,\,f_3)=H_3(f_1,\,f_2,\,f_3)\prod_{i=1}^{3}X(f_i). \tag{7}$$

$X(f)$ and $Y(f)$ are the discrete Fourier transform of $x(n)$ and $y(n)$, while $H_1(f)$, $H_2(f_1,\,f_2)$, and $H_3(f_1,\,f_2,\,f_3)$ are the one-, two-, and three-dimensional discrete Fourier transforms of $h_1(i)$, $h_2(i,\,j)$, and $h_3(i,\,j,\,k)$, respectively.

For any output frequency component f_o ($0\le f_o\le f_s-1/T$), the linear part of $Y_1(f_o)$ satisfies the well-known Shannon sampling theorem, hence, the output $Y_1(f_o)$ has no aliased components, but the quadratic part $Y_2(f_o)$ and the cubic part $Y_3(f_o)$ are obtained through the contraction operation as given by (4) and (5). Aliasing effects exist for these, and they may be assessed with the assistance of Figs. 1 and 2.

Fig. 1 presents an example to illustrate the contraction for the quadratic part in the case of a specific frequency component f_o of the output signal. All the frequency components from $f_2=-1/2T$ to $+1/2T$ are integrated in the Y_2-plane along the line $f_o=f_1+f_2$, and the frequency components from the first periodic extension in the Y_2-plane are contained in the integration path—this will lead to so-called "pseudoaliasing." For the cubically Volterra nonlinear system shown in Fig. 2, the aliasing occurs along the plane $f_o=f_1+f_2+f_3$ in a more complicated way. By referencing Figs. 1 and 2, if the aliasing effect is taken into account, the total output $Y(f_o)$ can be written as

$$Y(f_0)=Y_1(f_0)+Y_2(f_0)+Y_2(f_0-f_s)+Y_3(f_0-f_s)+Y_3(f_0)+Y_3(f_0+f_s). \tag{8}$$

From the above, it is seen that, for the identification of nonlinear systems band-limited to $|f_i|\le 1/2T$, it is sufficient

to sample the input and output signals at twice the maximum input frequency if the aliasing region is taken into consideration during the identification approach. However, for satisfactory identification, the bandwidth of the input signal should match the spectral range of the unknown system itself.

III. Mixed-Domain Volterra Model

In this section, a "mixed-domain" cubic Volterra model is described. The term "mixed-domain" comes from the fact that both time- and frequency-domain components are involved in the model. In the discrete time-domain, a Volterra-mapping-based cubically nonlinear model with finite memory length L can be represented as a truncated version of (1) as [8]

$$\begin{aligned} y(n) = &\sum_{i=0}^{L-1} h_1(i)x(n-i) + \sum_{i=0}^{L-1}\sum_{j=0}^{L-1} h_2(i,\,j)x(n-i)x(n-j) \\ &+ \sum_{i=0}^{L-1}\sum_{j=0}^{L-1}\sum_{k=0}^{L-1} h_3(i,\,j,\,k)x(n-i) \\ &\cdot x(n-j)x(n-k) + e(n). \end{aligned} \tag{9}$$

In order to determine the mixed-domain model, we define the input and output vectors, respectively, as [9]

$$x'_n = \Big[x'_n(0),\, x'_n(1),\, \ldots, x'_n(N-1)\Big]^T \tag{10}$$

$$y'_n = \Big[y'_n(0),\, y'_n(1),\, \ldots, y'_n(N-1)\Big]^T \tag{11}$$

where

$$x'_n(i) = x(n-i) \quad y'_n(i) = y(n-i). \tag{12}$$

Let the DFT of x'_n and y'_n be denoted by

$$X'_n = \Big[X'_n(0),\, X'_n(1),\, \ldots, X'_n(N-1)\Big]^T \tag{13}$$

$$Y'_n = \Big[Y'_n(0),\, Y'_n(1),\, \ldots, Y'_n(N-1)\Big]^T. \tag{14}$$

From the definition of the DFT, we can obtain

$$x'_n(i) = \frac{1}{N}\sum_{k=0}^{N-1} X'_n(k)w^{-ik} \quad X'_n(k) = \sum_{k=0}^{N-1} x'_n(i)w^{ik} \tag{15}$$

where $w = e^{-j(2\pi/N)}$.

Simultaneously, for the same set of data, we calculate the DFT of vectors

$$x = \Big[x(0),\, x(1),\, \ldots, x(N-1)\Big]^T \tag{16}$$

$$y = \Big[y(0),\, y(1),\, \ldots, y(N-1)\Big]^T. \tag{17}$$

The DFT of vectors x and y can be denoted, respectively, by

$$X = \Big[X(0),\, X(1),\, \ldots, X(N-1)\Big]^T \tag{18}$$

$$Y = \Big[Y(0),\, Y(1),\, \ldots, Y(N-1)\Big]^T. \tag{19}$$

By using (12) and (15), it is easy to show that

$$X'_n(k) = X^*(k)w^{kn} \quad Y'_n(k) = Y^*(k)w^{kn}. \tag{20}$$

Substituting (12) into (9) and assuming $L \le N$, we have

$$\begin{aligned} y(n) = &\sum_{i=0}^{N-1} h_1(i)x'_n(i) + \sum_{i=0}^{N-1}\sum_{j=0}^{N-1} h_2(i,\,j)x'_n(i)x'_n(j) \\ &+ \sum_{i=0}^{N-1}\sum_{j=0}^{N-1}\sum_{k=0}^{N-1} h_2(i,\,j)x'_n(i)x'_n(j)x'_n(k) + e(n). \end{aligned} \tag{21}$$

Substituting (15) into (21) and applying the multidimensional DFT of the Volterra kernels, we can obtain (22), shown at the bottom of this page, where $\overline{X}'_n(\cdot) = X'_n(\cdot)/N$, $y_L(n)$, $y_Q(n)$, and $y_C(n)$ represent the linear, quadratic, and cubic items, respectively. $H_1(\,)$, $H_2(,)$ and $H_3(,,)$, are the one-, two-, and three-dimensional DFT of $h_1(i)$, $h_2(i,\,j)$, and $h_3(i,\,j,\,k)$, respectively. Since (22) involves the time-domain output $y(n)$ together with the frequency-domain input $X'_n(\,)$, the described model in (22) is thus termed a mixed-domain model.

IV. Estimation Procedure of Volterra Kernels

In order to identify the Volterra model from (22) using a least-square solution technique under minimum sampling conditions, we need to obtain a more compact form of $y(n)$ by considering some symmetry properties of $X'_n(\,)$, $H_1(\cdot)$, $H_2(,)$, and $H_3(,,)$. Without loss of generality, all Volterra kernels in this

$$\begin{aligned} y(n) = &\underbrace{\sum_{p=-M+1}^{M} H_1^*(p)\overline{X}'_n(p)}_{y_L(n)} + \underbrace{\sum_{p=-M+1}^{M}\sum_{q=-M+1}^{M} H_2^*(p,\,q)\overline{X}'_n(p)\overline{X}'_n(q)}_{y_Q(n)} \\ &+ \underbrace{\sum_{p=-M+1}^{M}\sum_{q=-M+1}^{M}\sum_{r=-M+1}^{M} H_3^*(p,\,q,\,r)\overline{X}'_n(p)\overline{X}'_n(q)\overline{X}'_n(r)}_{y_C(n)} \end{aligned} \tag{22}$$

paper are assumed to be homogenous and, therefore, the associated transfer functions are symmetric and exhibit Hermitean symmetry [8], i.e.,

$$X_n(m) = X_n^*(-m) \tag{23}$$

$$Y_n(m) = Y_n^*(-m) \tag{24}$$

$$H_1(m) = H_1^*(-m) \tag{25}$$

$$h_2(i, j) = h_2(j, i) \tag{26}$$

$$H_2(p, q) = H_2(q, p) \tag{27}$$

$$H_2(p, q) = H_2^*(-p, -q) \tag{28}$$

$$H_3(p, q, r) = H_3^*(-p, -q, -r) \tag{29}$$

$$\begin{aligned} h_3(i, j, k) &= h_3(i, k, j) \\ &= h_3(j, i, k) \\ &= h_3(j, k, i) \\ &= h_3(k, i, j) \\ &= h_3(k, j, i) \end{aligned} \tag{30}$$

$$\begin{aligned} H_3(p, q, r) &= H_3(p, r, q) \\ &= H_3(q, p, r) \\ &= H_3(q, r, p) \\ &= H_3(r, p, q) = H_3(r, q, p) \end{aligned} \tag{31}$$

where "$*$" denotes complex conjugate.

Next, we consider a geometrical interpretation of the identification regions for the linear, quadratic, and cubic term of the mixed-domain Volterra model after the symmetry properties have been applied.

For the linear terms, by defining $L(p) = H_1^*(p)\overline{X}'_n(p)$, we have $L(-p) = L^*(p)$ Therefore, for $p \neq 0$ *or* M, we have $L(p) + L(-p) = 2\mathrm{Re}\{L(p)\}$, where $\mathrm{Re}\{r\}$ represents the real part of r. For $p = 0$ *or* M, $L(p)$ is itself real and, thus, $L(p) = \mathrm{Re}\{L(p)\}$. Finally, the linear part can be uniquely determined by $Re\{L(p)\}$, and $Y_L(n)$ can be written as

$$y_L(n) = \sum_{k=0}^{M} \mathrm{Re}\Big\{H_1^*(p)S_1(p)\Big\} = S_L^T H_L \tag{32}$$

where

$$S_1(p) = I_L(p)\overline{X}'_n(p) \tag{33}$$

$$I_L(p) = \begin{cases} 1, & \text{if } p = 0 \text{ or } M \\ 2, & \text{otherwise} \end{cases} \tag{34}$$

$$H_L = \Big[\mathrm{Re}\big\{H_1(0)\big\}\,\mathrm{Re}\big\{H_1(1)\big\}\,\mathrm{Im}\big\{H_1(1)\big\} \cdots \mathrm{Re}\big\{H_1(M)\big\}\Big]^T \tag{35}$$

$$S_L = \Big[\mathrm{Re}\big\{S_1(0)\big\}\,\mathrm{Re}\big\{S_1(1)\big\}\,\mathrm{Im}\big\{S_1(1)\big\} \cdots \mathrm{Re}\big\{S_1(M)\big\}\Big]^T. \tag{36}$$

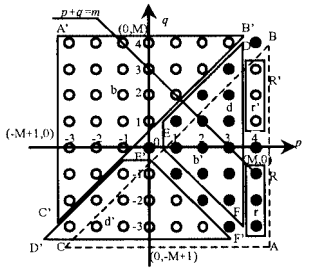

Fig. 3. Effect of the symmetry properties $Q(p, q) = Q(q, p), Q(-p, -q) = Q^*(q, p)$, and $Q(M, q) = Q^*(M, -q)$ on the two-dimensional frequency plane.

For $p = 0$ *or* M, $H_1(p)$ and $S_1(p)$ is itself real, thus the corresponding imaginary part is removed from H_L and S_L, respectively, of which the dimensional number is $N_L = 2M \times 1$.

For the quadratic terms, using the (p, q)-plane for the eight-point DFT $(N = 8, M = 4)$ case as an aid, as shown in Fig. 3, and defining $Q(p, q) = H_2^*(p, q)\overline{X}'_n(p)\overline{X}'_n(q)$, we have

$$Q(p, q) = Q(q, p) \tag{37}$$

$$Q(-p, -q) = Q^*(q, p) \tag{38}$$

$$Q(M, q) = Q^*(M, -q). \tag{39}$$

After taking into account the above symmetry properties, the quadratic part $y_Q(n)$ can be uniquely determined by $\mathrm{Re}\{Q(p, q)\}$ for those $Q(p, q)$'s denoted by black dots in Fig. 3, and can be written as

$$y_Q(n) = \sum_{(p,q)\in U} \mathrm{Re}\big\{H_2^*(p, q)S_2(p, q)\big\} = S_Q^T H_Q \tag{40}$$

$$S_2(p, q) = I_Q(p, q)\overline{X}'_n(p)\overline{X}'_n(q) \tag{41}$$

$$I_Q(p, q) = \begin{cases} 1, & p = q = 0 \text{ or } p = q = M \\ 2, & (p, q) = (M, 0) \text{ or } (p = |q|,\ p \neq 0, M) \\ 4, & \text{otherwise} \end{cases} \tag{42}$$

$$H_Q = \Big[H_{2r}^{(0)T} H_{2r}^{(1)T} H_{2i}^{(1)T} \cdots H_{2r}^{(M)T} \cdots H_{2r}^{(N-1)T} H_{2i}^{(N-1)T} H_{2r}^{(N)T}\Big]^T \tag{43}$$

$$S_Q = \Big[S_{2r}^{(0)T} S_{2r}^{(1)T} S_{2i}^{(1)T} \cdots S_{2r}^{(M)T} \cdots S_{2r}^{(N-1)T} S_{2i}^{(N-1)T} S_{2r}^{(N)T}\Big]^T \tag{44}$$

where $\boldsymbol{U}$ is the set of the points denoted by the black dots in Fig. 3. In (43) and (44), $H_2^{(m)} = H_{2r}^{(m)} + iH_{2i}^{(m)}$, and $S_2^{(m)} = S_{2r}^{(m)} + iS_{2i}^{(m)}$ for $m = 0, 1, \ldots N$ can be defined as

$$H_2^m = \big[H_2(k_o, m - k_o)\ H_2(k_o + 1, m - k_o - 1) \cdots H_2(k_M, m - k_M)\big]^T \tag{45}$$

$$S_2^m = \big[S_2(k_o, m - k_o)\ S_2(k_o + 1, m - k_o - 1) \cdots S_2(k_M, m - k_M)\big]^T \tag{46}$$

where $k_o = \lfloor (m + 1/2) \rfloor$ with $\lfloor r \rfloor$ denoting the largest integer being less or equal to r, and $k_M = M - 1$ for $m = 0$ or

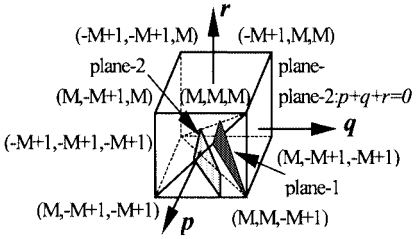

Fig. 4. Counting region for cubic terms.

$M < m < N$, $k_M = M$ otherwise. It should be noted that $H_2(M, 0)$, $H_2^{(0)}$, $H_2^{(N)}$, $S_2(M, 0)$, $S_2^{(0)}$, and $S_2^{(N)}$ are themselves real and, thus, the corresponding imaginary parts are removed from H_Q and S_Q, respectively. The dimensional numbers of H_Q and S_Q are then $N_Q = M(2M+1) \times 1$.

By defining $C(p, q, r) = H_3^*(p, q, r)\,\overline{X}'_n(p)\overline{X}'_n(q)\overline{X}'_n(r)$ for the cubic terms, we have

$$\begin{aligned} C(p, q, r) &= C(p, r, q) \\ &= C(q, p, r) \\ &= C(q, r, p) \\ &= C(r, p, q) \\ &= C(r, q, p) \end{aligned} \tag{47}$$

$$C(M, M, r) = C^*(M, M, -r) \tag{48}$$

$$C(p, q, r) = C^*(-q, -p, -r) \tag{49}$$

$$C(M, q, r) = C^*(M, -q, -r). \tag{50}$$

Using the cube in three-dimensional space (p, q, r) as an aid, as shown in Fig. 4, after taking into account the properties of (47), the counting region for the cubic terms is reduced to one-sixth of the cube with a summation to the plane of $m = p+q+r$ with $-M+1 \le p, q, r \le M$, $r \le q \le p$, and $0 \le m \le 3M$. For example, planes-1 and plane-2 in Fig. 4 describe the counting plane for the cubic terms in the condition of $m = 0$ and $m = M$, respectively.

In order to describe the Hermitean symmetry properties of the cubic terms, we use the (p, q, r) three-dimensional cube for an eight-point DFT ($N = 8$, $M = 4$) case as an aid. We then cut the counting region shown in Fig. 4 into $\boldsymbol{N}$ pieces along the p-axis, as shown in Fig. 5.

After taking into account the above symmetry properties, the cubic parts $y_C(n)$ can be uniquely determined by $\mathrm{Re}\{C(p, q, r)\}$ for those $C(p, q, r)$'s denoted by the black dots marked by the line of $m = 0, 1, 2, \ldots 3M$ in Fig. 5 and can be written as

$$\begin{aligned} y_C(n) &= \sum_{(p, q, r) \in U} \mathrm{Re}\{H_3^*(p, q, r) S_3(p, q, r)\} \\ &= S_C^T H_C \end{aligned} \tag{51}$$

$$S_3(p, q, r) = I_C(p, q, r) J_C(p, q, r) \tag{52}$$

$$I_C(p, q, r) = \begin{cases} 6, & \text{if } (p \ne q),\ (q \ne r),\ \text{and } (p \ne r) \\ 3, & \text{otherwise} \\ 1, & \text{if } (p = q = r) \end{cases} \tag{53}$$

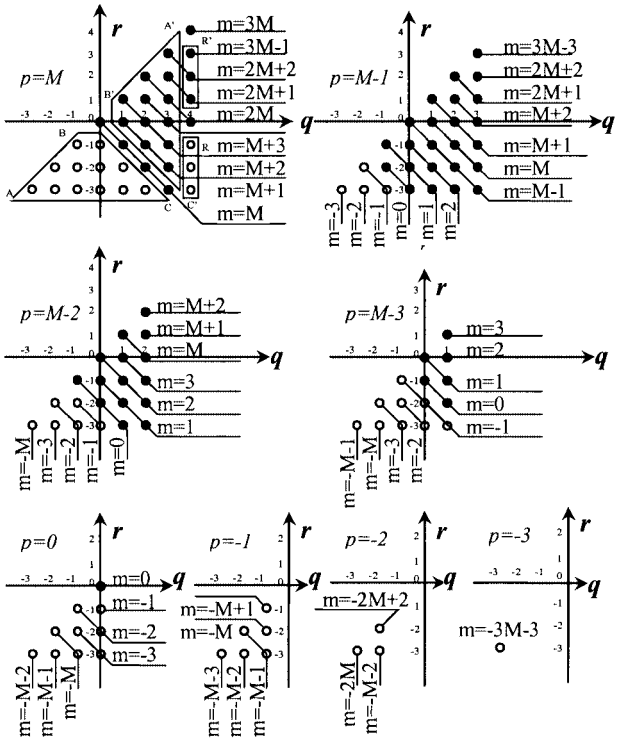

Fig. 5. Effect of Hermitean symmetry properties in the case of the cubic terms for a DFT of dimension $N = 8$.

$$J_C(p, q, r) = \begin{cases} 1, & \text{if } m = 0 \text{ and } m = 3M \\ 2, & \text{otherwise} \end{cases} \tag{54}$$

$$\begin{aligned} H_C = \Big[& H_{3r}^{(0)T} H_{3i}^{(0)T} \cdots H_{3r}^{(M)T} \cdots H_{3r}^{(2M)T} \\ & \cdots H_{3r}^{(3M)T} \Big]^T \end{aligned} \tag{55}$$

$$\begin{aligned} S_C = \Big[& S_{3r}^{(0)T} S_{3i}^{(0)T} \cdots S_{3r}^{(M)T} \cdots S_{3r}^{(2M)T} \\ & \cdots S_{3r}^{(3M)T} \Big]^T \end{aligned} \tag{56}$$

where U is the set of the points denoted by the black dots marked by the line of $m = 0, 1, 2, \ldots 3M$ in Fig. 5. $H_3^{(m)} = H_{3r}^{(m)} + iH_{3i}^{(m)}$ and $S_3^{(m)} = S_{3r}^{(m)} + iS_{3i}^{(m)}$ for $m = 0, 1, 2, \ldots 3M$ can be defined as

$$H_3^{(m)} = \begin{bmatrix} H_3(l_0, l_1, m - l_0 - l_1) \\ \vdots \\ H_3(l_0, k_1, m - l_0 - k_1) \\ \vdots \\ H_3(l_0 - 1, l_1, m - l_0 - l_1 + 1) \\ \vdots \\ H_3(l_0 - 1, k_1, m - l_0 - k_1 + 1) \\ \vdots \\ H_3(k_0, k_1, m - k_0 - k_1) \end{bmatrix} \tag{57}$$

$$S_3^{(m)} = \begin{bmatrix} S_3(l_0, l_1, m-l_0-l_1) \\ \vdots \\ S_3(l_0, k_1, m-l_0-k_1) \\ \vdots \\ S_3(l_0-1, l_1, m-l_0-l_1+1) \\ \vdots \\ S_3(l_0-1, k_1, m-l_0-k_1+1) \\ \vdots \\ S_3(k_0, k_1, m-k_0-k_1) \end{bmatrix} \tag{58}$$

where $l_0 = \lfloor (m+2/3) \rfloor$ with $\lfloor r \rfloor$ denoting the largest integer being less or equal to r, and $k_0 = M-1$ for $m < M$, $k_0 = M$ otherwise; $l_1 = \lfloor (m-p+1/2) \rfloor$ and $k_1 = p - r[2p-m-k_0] - \lambda$ where

$$r[2p-m-k_0] = \begin{cases} 2p-m-k_0, & \text{if } (2p-m-k_0) \geq 0 \\ 0, & \text{if } (2p-m-k_0) < 0 \end{cases}$$

and

$$\lambda = \begin{cases} 1, & M \leq m < 2M \text{ and } p = M \\ 0, & \text{otherwise.} \end{cases}$$

Specially note that $H_3(p, 0, -p)$, $H_3(M, q, -q)$, $H_3(M, M, 0)$, $H_3(M, M, M)$, $S_3(p, 0, -p)$, $S_3(M, q, -q)$, $S_3(M, M, 0)$, and $S_3(M, M, M)$ are themselves real, thus, the corresponding imaginary parts are removed from H_C and S_C, respectively. Therefore, the dimensional numbers of H_C and S_C are $N_C = 2[(k_1-l_1+1)(k_o-l_o+1)-(M+1)] \times 1$.

Finally, by considering (32), (40), and (51), we can obtain

$$y(n) = X^T H \tag{59}$$

where

$$H = \left[H_L^T, H_Q^T, H_C^T \right]^T \tag{60}$$

$$X = \left[S_L^T, S_Q^T, S_C^T \right]^T. \tag{61}$$

The total of unknown variables in (59) is $N_L+N_Q+N_C$, but by using the DFT of N, we can set up only N equations from the expansion (59). In order to solve H, the input $x(n)$ should have at least $\lfloor (N_L+N_Q+N_C)/N \rfloor \times N$ general random input data so that the argument matrix of $\boldsymbol{X}$ is a nonsingular matrix. In this way, we can apply a least squares method to solve the equation, and find the solution for the cubic Volterra transfer functions H_L, H_Q and H_C. The time-domain Volterra kernels can then be obtained from the appropriate inverse DFTs. Although the details of a Volterra kernel model up to third order have been addressed here, the methodology itself in not limited to a third-order Volterra model and is straightforward to extend to higher order Volterra models.

V. Computer Simulation

A software tool combining Visual C++ and MATLAB has been developed to implement and verify the above approach and the software has been used to evaluate a range of known cubically nonlinear systems. Excellent agreement has been obtained between identified and theoretical kernels in all cases. Some verification examples may be found in the authors' previous publications [13]–[16]. Here, the two examples particularly emphasize applications to high frequencies.

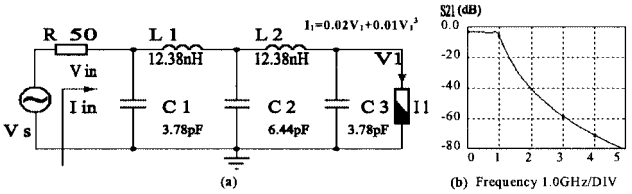

Fig. 6. Low-pass filter with nonlinear termination.

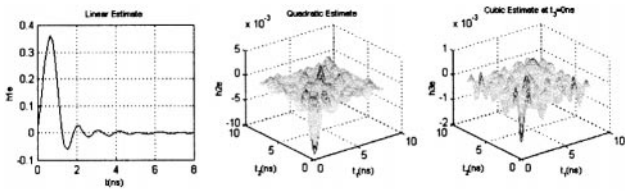

Fig. 7. Estimated first-, second-, and third-order ($t_3 = 0$–1.5 ns) Volterra kernel of the low-pass filter with nonlinear termination.

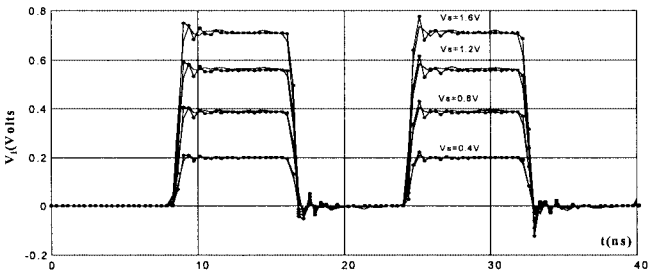

Fig. 8. Comparison between results from SPICE (•) and results from the present method using multidimensional convolutions on Volterra kernels.

As shown in Fig. 6(a), the first example involves a lumped-element low-pass filter terminated by a voltage-controlled nonlinear load resistance defined by the function of $i = 0.02v + 0.01v^3$. The filter's linear transfer characteristics under 50-Ω load termination is shown in Fig. 6(b).

Fig. 7 shows the Volterra kernels that are obtained by the proposed method with a 3-GHz sampling frequency using a multitone excitation and a 32-point DFT technique. Due to space limitations, the third-order kernels are sliced along the t_3-time axis and only one item of $t_3 = 0$ is shown in Fig. 7.

The identified Volterra kernels can be used within a time-domain simulation to obtain the time-domain response to any arbitrary excitation. The output voltage waveforms compared in Fig. 8 are obtained from the SPICE simulator and from multidimensional convolution operations using the above kernels when the system is excited by an input of 8-ns pulsewidth and 125-ps rise and fall times at different pulse amplitudes.

In the second example, an experimental hybrid power amplifier was designed and fabricated to verify the previously described modeling method by comparing the measured and predicted behavior of a bipolar junction transistor (BJT) RF power amplifier under excitation by an IS-95 CDMA signal. Fig. 9

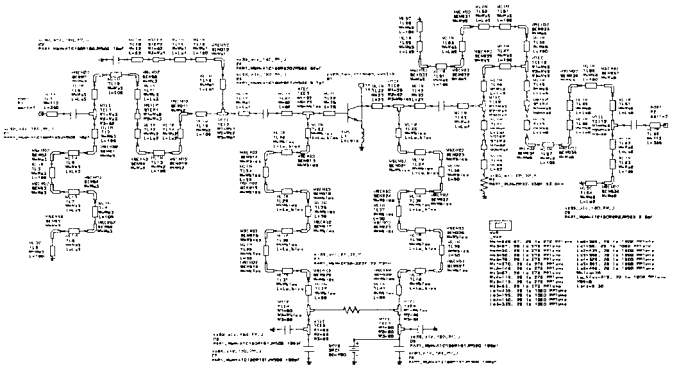

Fig. 9. Schematic diagram of hybrid test amplifier.

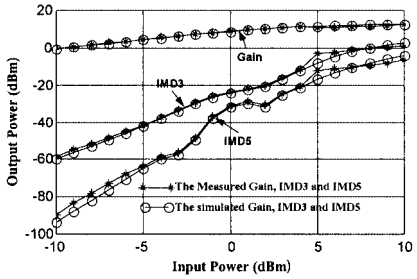

Fig. 10. Comparison of measured and calculated intermodulation nonlinearities.

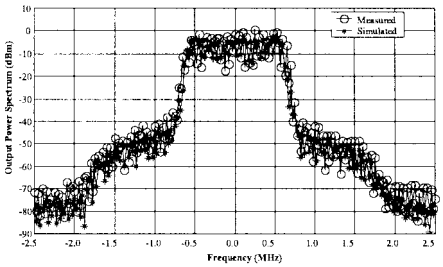

Fig. 11. Measured and simulated output power spectrum.

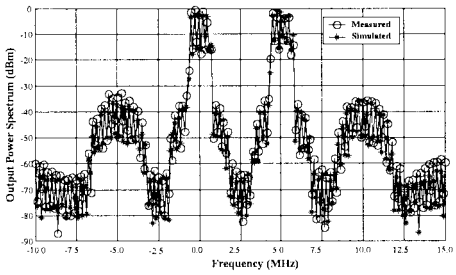

Fig. 12. Measured and calculated intermodulation spectrum.

gives the schematic of the amplifier. The active component used in the power amplifier was an HP-AT42085 bipolar transistor with parameters $P\mathrm{diss} = 500$ mW, $Ic = 35$ mA, and $VCC = 8$ V.

Fig. 10 shows the measured and calculated results of fundamental and intermodulation performance at the frequency point of 1.8 GHz. The frequency separation between the two tones is 1 MHz. Fig. 11 shows a comparison of the measured and simulated output power spectrum of the power amplifier under a IS-95 CDMA signal excitation. Fig. 12 shows the measured and simulated output power spectrum of the power amplifier excited by two passband CDMA signals with 5-MHz offset centered on 1.8025 GHz. In Fig. 11 and Fig. 12, the resolution bandwidth of the spectrum analyzer is set to 3 kHz and the frequency axis is normalized by applying an 1800-MHz frequency offset, i.e., the 0.0 Hz represents 1800 MHz. As can be seen, the intermodulation products are broadened to roughly three times the bandwidth of the CDMA signals themselves.

VI. Conclusions

This paper has described an efficient and accurate method for the estimation of Volterra kernels for a nonlinear system. As the above examples have shown, favorable agreement has been obtained in a range of validation studies undertaken of the proposed modeling method. This paper has also shown that the Volterra representation can successfully predict nonlinear intermodulation distortions, especially in the case of the nonlinear characteristics of a microwave power amplifier. The Volterra description generally works well for a power amplifier if the input power level is not increased much beyond the 1-dB compression input power level. Furthermore, being a descriptive black-box-type model of the system, this kind of representation is also capable of efficiently predicting the amplifier's output spectrum when driven by multiple digitally modulated communication signals. Simulations of this kind are difficult to undertake using other available methods. This makes it possible for the amplifier designer to select the appropriate power component and for the communication system designer to consider the effects of impairments such as adjacent channel interference and cross-modulation.

References

[1] W. Anzil and T. Melander, "Radio architecture of a wide-band DS-CDMA tested for future cellular systems," in *IEEE MTT-S Int. Microwave Symp. Dig.*, 1997, pp. 1387–1390.

[2] O. K. Jensen *et al.*, "RF receiver requirement for 3G W-CDMA mobile equipment," *Microwave J.*, vol. 43, no. 2, pp. 22–46, Feb. 2000.

[3] J. Verspecht *et al.*, "System level simulation benefits from frequency domain behavioral models of mixers and amplifiers," in *Proc. 29th Eur. Microwave Conf.*, vol. 2, Munich, Germany, Oct. 1999, pp. 29–32.

[4] Q. J. Zhang and K. C. Gupta, *Neural Networks for RF and Microwave Design*. Boston, MA: Artech House, 2000.

[5] E. Root, "On table-based device models," presented at the IEEE MTT-S Int. Microwave Symp. Workshop, 1997.

[6] S. Im and E. J. Powers, "Extended principal domain for Volterra models," in *Proc. IEEE Signal Processing ATHOS High-Order Statistics Workshop*, Begur, Girona, Spain, 1995, pp. 381–385.

[7] K. I. Kim and E. J. Powers, "A digital method of modeling quadratically nonlinear system with a general random input," *IEEE Trans. Acoust., Speech, Signal Processing*, vol. 36, pp. 1758–1769, Nov. 1988.

[8] W. Nam and E. J. Powers, "Application of higher order spectral analysis to cubically nonlinear system identification," *IEEE Trans. Signal Processing*, vol. 42, pp. 1746–1765, July 1994.

[9] C.-H. Tseng, "A mixed-domain method for identification of quadratically nonlinear systems," *IEEE Trans. Signal Processing*, vol. 45, pp. 1013–1024, Apr. 1997.

[10] J. Redfern and G. T. Zhou, "Performance analysis of Volterra kernel estimators with Gaussian inputs," in *Proc. IEEE MTT-S Int. Microwave Symp. Dig.*, 1997, pp. 162–165.

[11] H. I. Krausz, "Identification of nonlinear systems using random impulse train inputs," in *Biological Cybernetics*. Berlin, Germany: Springer-Verlag, 1975, vol. 19, pp. 217–230.

[12] L. O. Chua and C. Y. Ng, "Frequency-domain analysis of nonlinear systems: Formulation of transfer function," *Electron. Circuits Syst.*, vol. 3, pp. 257–269, 1979.

[13] T. H. Wang and T. J. Brazil, "A mixed-domain modeling method for microwave nonlinear systems and semiconductor devices in high frequency applications," in *28th Eur. Microwave Conf.*, vol. 2, Amsterdam, The Netherlands, 1998, pp. 129–134.

[14] T. H. Wang and T. J. Brazil, "A Volterra mapping-based S-parameter behavioral model for nonlinear RF and microwave circuits and systems," in *IEEE MTT-S Int. Microwave Symp. Dig.*, vol. 2, Anaheim, CA, June 1999, pp. 783–786.

[15] T. Wang and T. J. Brazil, "The estimation of Volterra transfer functions with applications to RF power amplifier behavior evaluation for CDMA digital communication," in *IEEE MTT-S Int. Microwave Symp. Dig.*, vol. 2, Boston, MA, June 2000, pp. 425–428.

[16] ——, "Using Volterra mapping based behavioral model to evaluate the ACI and cross modulation in CDMA communication systems," in *Proc. 5th IEEE High Frequency Postgraduate Colloq.*, Dublin, U.K., Sept. 7–8, 2000, pp. 102–108.

Tianhai Wang (M'01) was born in Hebei, China, in 1966. He received the M.E. and B.E. degrees in electronic engineering from Tianjin (PeiYang) University, Tianjin, China, in 1991 and 1988, respectively, and the Ph.D. degree in electronic and electrical engineering from University College Dublin, Dublin, U.K., in 2000.

From March 1991 to March 1997, he was with the Department of Electronic Engineering, Tianjin University, as an Assistant Lecturer then a Lecturer. Since March 1997, he has been with the Microwave Research Group, Department of Electronic and Electrical Engineering, University College Dublin. He is currently a Senior Electrical Engineer with the Corporate Research and Design Department, M/A-COM Inc., Tycoelectronics, Lowell, MA. His research interests are nonlinear circuit analysis and CAD, nonlinear digital signal processing (DSP) algorithm, monolithic-microwave integrated-circuit (MMIC) designs, power-amplifier modeling, and linearization for wireless communication application.

Thomas J. Brazil (M'86–SM'02) was born in County Offaly, U.K. He received the B.E. degree in electrical engineering from University College Dublin (UCD), Dublin, U.K., in 1973, and the Ph.D. degree from the National University of Ireland, Galway, U.K., in 1977.

He was subsequently involved with microwave subsystem development with Plessey Research, Caswell, U.K., and was a Lecturer with the Department of Electronic Engineering, University of Birmingham, Birmingham, U.K. In 1980, he returned to UCD, where he is currently a Professor of electronic engineering and Head of the Department of Electronic and Electrical Engineering. His research interests are in the fields of nonlinear component and system modeling and device characterization techniques, including applications to a wide range of microwave transistor devices. He also has interests in nonlinear simulation algorithms and several areas of microwave subsystem design and applications.